• Original Paper •

Main Energy Paths and Energy Cascade Processes of the Two Types of Persistent Heavy Rainfall Events over the Yangtze River–Huaihe River Basin

Yuanchun ZHANG[1], Jianhua SUN[*1,2], and Shenming FU[3]

[1]*Key Laboratory of Cloud-Precipitation Physics and Severe Storms, Institute of Atmospheric Physics,*
Chinese Academy of Sciences, Beijing 100029, China
[2]*University of Chinese Academy of Sciences, Beijing 100049, China*
[3]*International Center for Climate and Environment Sciences, Institute of Atmospheric Physics,*
Chinese Academy of Sciences, Beijing 100029, China

ABSTRACT

Two types of persistent heavy rainfall events (PHREs) over the Yangtze River–Huaihe River Basin were determined in a recent statistical study: type A, whose precipitation is mainly located to the south of the Yangtze River; and type B, whose precipitation is mainly located to the north of the river. The present study investigated these two PHRE types using a newly derived set of energy equations to show the scale interaction and main energy paths contributing to the persistence of the precipitation. The main results were as follows. The available potential energy (APE) and kinetic energy (KE) associated with both PHRE types generally increased upward in the troposphere, with the energy of the type-A PHREs stronger than that of the type-B PHREs (except for in the middle troposphere). There were two main common and universal energy paths of the two PHRE types: (1) the baroclinic energy conversion from APE to KE was the dominant energy source for the evolution of large-scale background circulations; and (2) the downscaled energy cascade processes of KE and APE were vital for sustaining the eddy flow, which directly caused the PHREs. The significant differences between the two PHRE types mainly appeared in the lower troposphere, where the baroclinic energy conversion associated with the eddy flow in type-A PHREs was from KE to APE, which reduced the intensity of the precipitation-related eddy flow; whereas, the conversion in type-B PHREs was from APE to KE, which enhanced the eddy flow.

Key words: persistent heavy rainfall event, energy cascade process, large-scale background circulation, precipitation-related eddy flow

1. Introduction

The Yangtze River–Huaihe River valleys often suffer persistent heavy rainfall events (PHREs) in the warm season. The related severe flooding events cause large economic, life, and property losses, such as the well-known Yangtze River flood events in 1998 and 1999 (Tao et al., 2001, 2004, Zhao et al., 2004), and the notable Huaihe River flood events in 1991, 2003 and 2007 (Ding, 1993; Zhao et al., 2004). Previous studies have found that large-scale circulation stability is essential for the persistence of heavy precipitation (Tao and Xu, 1962), and thus they proposed that a proper classification of the large-scale circulation patterns is vital for forecasting and understanding PHREs. Previous studies have

classified PHREs into different types according to different motivations. For instance, Tang et al. (2006) pointed out that the PHREs they selected could be classified into five categories according to their intensity, into three types according to their circulation regime, and into eight groups according to the geographic locations of their rainbands. Xu (2008) applied EOF analysis to divide the PHREs in South China into three modes: consistent, transmeridional alternate, and latitudinal opposition. Most recently, Wang et al. (2014) utilized daily precipitation data from 752 stations in China to classify the PHREs over South China. Using the objective pattern correlation method, they classified PHREs in the Yangtze River–Huaihe Rriver valley into three basic types: type A, with the main rainbelt located to the south of the Yangtze River; type B, with the main rainbelt located to the north of the Yangtze River; and type C, with the main rainbelt stretched along the Yangtze River. Based on this classification system, a com-

---

* Corresponding author: Jianhua SUN

  Email: sjh@mail.iap.ac.cn

posite study was conducted to show the main similarities and differences among the three PHRE types.

The mechanisms accounting for the persistence of precipitation is a critical topic. Energetics, including the available potential energy (APE) and kinetic energy (KE), has been effectively employed in PHRE-related studies (Fu et al., 2011, 2013; Guo et al., 2012). Of these, some studies have tried to clarify the energy conversion between the precipitation-related eddy flow and its background circulation (mean flow). For instance, Chen et al. (1990) used horizontal filtering to diagnose the scale interaction that transferred KE from synoptic-scale systems to mesoscale systems. Ritchie and Holland (1997) proposed that scale interactions of energy resulted in favorable conditions for storm development. Li (2007) showed that the energy conversion from a synoptic scale disturbance to the low-frequency fluctuation was obviously enhanced in the middle and lower troposphere during the heavy rainfall. Fu et al. (2015) analyzed a long-lived mesoscale vortex and found that the downscaled energy cascade process (ECP) of KE was the key factor for sustaining this heavy precipitation vortex. Li and Li (2016) found that the energy conversion between the eddy flow and its background circulation contributed to the development of the precipitation systems during a heavy rainfall event. As mentioned above, although previous studies have shown that the scale interactions of energy can affect a heavy rainfall event significantly, the specific mechanisms underlying the interactions between the precipitation-related eddy flow and its background circulation have rarely been discussed. Moreover, for PHREs over the Yangtze River–Huaihe River valleys, the mechanisms dominating their persistence and the main energy paths of different scale weather systems remain unclear. Therefore, based on the classification of PHREs from Wang et al. (2014), this study was conducted to address these two points.

The paper is structured as follows. The data and methodology are introduced in section 2. Section 3 provides an overview of the selected PHREs. A comparison of the energy features and paths of the PHRE types are summarized in section 4. Finally, a conclusion and discussion is provided in section 5.

2. Data and methodology

2.1. *Data*

Six-hourly NCEP CFSR data ($0.5° \times 0.5°$) (Saha et al., 2010) were used for the synoptic analysis and energy calculations in this study. Using daily precipitation data from 752 meteorological stations in China (interpolated into $0.25° \times 0.25°$ grids based on the Cressman objective method), Wang et al. (2014) classified the PHREs over the Yangtze River–Huaihe Rriver basin into three basic types: type A (main rainbelt located south of the Yangtze River); type B (main rainbelt located north of the Yangtze River); and type C (main rainbelt located along the Yangtze River). Of these three types, type A and type B show significant differences in their

precipitation distribution, circulation patterns and influencing systems, while type C mainly shows hybrid features of type A and type B. Moreover, type A and type B show a more stable maintenance state than type C. Therefore, the present study primarily focused on types A and B; the features of type-C PHREs are presented in the conclusion and discussion (section 5). The former two types were compared in detail to understand the fundamental energy characteristics governing the PHREs over the Yangtze River–Huaihe River basin.

2.2. *Methodology*

According to the Fourier series, a meteorological variable can be decomposed into a mean part and a perturbation part, i.e., $b = \bar{b} + b'$, where b is a sample variable, the overbar represents a time-mean operator (mean or running mean), and the prime represents a perturbation operator. The perturbation part is the direct trigger for a PHRE, and the mean part acts as the background for the variation of the perturbation. As APE and KE are key factors during a PHRE (Fu et al., 2013), they were analyzed in detail to determine the respective fundamental mechanisms sustaining the type-A and type-B PHREs. Eight PHRE cases persisting for about three days (four cases of each type) were selected to study the energy characteristics of type-A and -B PHREs. Because all eight PHRE cases persisted for approximately three days [Table 1; these cases are also shown in Table 5 of Wang et al. (2014)], a time window of 72 h was used to conduct the temporal scale separation (calculating the mean or running mean). After separation, the flow was decomposed into a perturbation part (eddy flow) with the period below 72 h, and its background circulation (mean flow). Then, the interaction between the precipitation-related eddy flow and its background circulation was investigated using the energy diagnostic scheme from Murakami (2011):

$$\partial A_{\mathrm{M}}/\partial t = G(A_{\mathrm{M}}) - C(A_{\mathrm{M}}, K_{\mathrm{M}}) - C(A_{\mathrm{M}}, A_{\mathrm{I}})$$
$$- B(A_{\mathrm{M}}) + R(A_{\mathrm{M}}), \tag{1}$$

$$\partial K_{\mathrm{M}}/\partial t = C(A_{\mathrm{M}}, K_{\mathrm{M}}) - C(K_{\mathrm{M}}, K_{\mathrm{I}}) - D(K_{\mathrm{M}}) - B(K_{\mathrm{M}}), \tag{2}$$

$$\partial \overline{A_{\mathrm{T}}}/\partial t = G(\overline{A_{\mathrm{T}}}) - C(\overline{A_{\mathrm{T}}}, \overline{K_{\mathrm{T}}}) - C(\overline{A_{\mathrm{T}}}, A_{\mathrm{I}}) - B(\overline{A_{\mathrm{T}}}), \tag{3}$$

$$\partial \overline{K_{\mathrm{T}}}/\partial t = C(\overline{A_{\mathrm{T}}}, \overline{K_{\mathrm{T}}}) - C(\overline{K_{\mathrm{T}}}, K_{\mathrm{I}}) - D(\overline{K_{\mathrm{T}}}) - B(\overline{K_{\mathrm{T}}}). \tag{4}$$

Here, A_{M}, A_{I} and A_{T} are the time-mean, interaction and perturbation APE, respectively; and K_{M}, K_{I} and K_{T} are the time-mean, interaction and perturbation KE, respectively. The terms $G(A_{\mathrm{M}})$ and $G(\overline{A_{\mathrm{T}}})$ are the diabatic generation or extinction of A_{M} and A_{T}. $C(X1, X2)$ represents the conversion between the energy $X1$ and energy $X2$. $D(K_{\mathrm{M}})$ and $D(\overline{K_{\mathrm{T}}})$ denote the dissipation of K_{M} and K_{T}. $B(X)$ is the three-

Table 1. Three-day consecutive rainfall events of type-A and type-B PHREs.

Type A	Type B
June 29 to July 1 1989	June 12 to June 14 1991
June 12 to June 14 1994	July 2 to July 4 1996
June 19 to June 21 1998	June 21 to June 23 2002
June 9 to June 11 2000	July 3 to July 5 2007

dimensional transport associated with X. $R(A_M)$ represents the vertical transport of heat. Unlike traditional energy budget systems (Holopainen, 1978; Plumb, 1983), the energy budget used in this study has an interaction APE term (A_I) and an interaction KE term (K_I). These two new types of energy act as a linkage between the mean energy and perturbation energy, which remove the ambiguity associated with the energy conversion in traditional local energy diagnostic schemes (Holopainen, 1978; Plumb, 1983). For details of the energy budget system used in this study, please refer to Murakami et al. (2011), Murakami et al. (2011) and Fu et al. (2016).

3. Overview of the PHREs

A total of eight PHREs were selected in this study—four type A cases and four type B cases (Table 1), all of which lasted for three days. These events all appeared between June and July, and most of them occurred during the typical mei-yu period (15 June–15 July). The three-day averaged 850 hPa perturbation KE and the corresponding three-day accumulated precipitation are shown in Fig. 1. The location, orientation and distribution of the accumulated precipitation were highly consistent with the perturbation KE, which implies the perturbation was the direct trigger for the PHREs and the perturbation KE can be used as an effective indicator for the precipitation-related eddy flow. To show the overall feature of the precipitation-related eddy flow, an area mean was calculated. Following the definition of the key region (green box in Fig. 2) in Wang et al. (2014), the energy budget terms of the type-A PHREs were averaged within the south box (south of the Yangtze River) [(26°–30°N, 112°–122.5°E); key area for type A (KA-A); Fig. 3], and those of the type-B PHREs were averaged within the north box [(30°–34°N, 112°–122.5°E); key area for type B (KA-B); Fig. 3].

3.1. Comparison of the background circulation in type-A and -B PHREs

Generally, during each of the eight selected PHREs, the background circulation maintained quasi-stationarity (not shown). This provided favorable conditions for the sustainment of the PHREs. Figure 2 shows the 3-day averaged geopotential height and temperature at 850 hPa of each case. For type A (left column in Figs. 2 and 3), though the circulation at high latitude varied among the four cases, a low trough covered East China and the key area was located in the regions from the rear to the base of this trough. The northwesterlies behind the trough and the southwesterlies along the northwestern edge of the western Pacific subtropical high (WPSH) converged over KA-A, corresponding with the stronger positive vorticity at 850 hPa (Fig. 3, left column). However, the circulation distribution of the cases in 1989 and 2000 showed larger meridional amplitudes at 500 hPa and stronger convergence at 850 hPa than the other two cases. For type B (right column in Figs. 2 and 3), the WPSH landed to the areas south of the Yangtze River and weak ridges cov-

ered the mid–high latitudes. The circulation distribution featured small meridional amplitudes. KA-B in the four cases was ahead of the ridges (Fig. 2), with the convergence belt situated north of the Yangtze River.

3.2. Composite features of the background circulation in type-A and -B PHREs

To show the respective common features for the type-A and -B PHREs' background circulations, separate composites for the four type-A and four type-B cases were produced (Figs. 4 and 5). For the type-A PHREs, the geopotential height at 200 hPa showed a typical two trough and one ridge pattern in the middle to high latitudes (Fig. 4a): the western low trough was located over Lake Balkhash, the eastern trough extended from North China to the lower reaches of the Yangtze River, and the ridge in the middle covered the region south of Lake Baikal. The South Asia high dominated the whole of the low latitudes. KA-A was beneath the south part of the western trough and the northeastern part of the South Asia high. The upper-level jets mainly persisted between 30°N and 45°N. For the type-B PHREs, the 200 hPa circulation was obviously flatter than that in type A, with a straight westerly flow persisting in the middle and high latitudes and a weak ridge located at approximately 110°E, covering North China. The upper-level jets covered the area between 35°N and 45°N, which was to the north of the 200 hPa jet in the type-A PHREs. The South Asia high was stronger and wider than in the type-A PHREs, and extended northward to approximately 30°N. KA-A was located in the northeast quadrant of the South Asia high (Fig. 4b). The 500 hPa geopotential height in the type-A and -B PHREs in the middle to high latitudes showed a similar pattern to that at 200 hPa. KA-A was governed by the northwesterly wind, and the 5880 gpm isohypse of the WPSH covered the area east of 120°E and south of 30°N. The westerly wind governed KA-B PHREs and the subtropical high covered KA-B. At lower levels, the northeast–southwest oriented convergence belt in the type-A PHREs was located south of the Yangtze River, corresponding to a potential temperature trough with a strong temperature gradient (Figs. 5a and c), which meant that the baroclinicity was strong. In contrast, the convergence belt of the type-B PHREs was mainly orientated in the west–east direction and extended north of the Yangtze River. It was weaker than that in the type-A PHREs, and located at the north edge of the high potential temperature region (Figs. 5b and d).

4. Energy features of the two types of PHREs

As shown in Fig. 1 and Figs. 5c and d, in both of the four-case composites for the type-A and -B PHREs, the lower-level three-day averaged K_T band corresponded closely to the convergence and cyclonic vorticity band (low-level wind shear or mei-yu front). This confirms that the stably persistent perturbation KE band acted as a direct trigger for the selected PHREs. Therefore, a thorough analysis of how
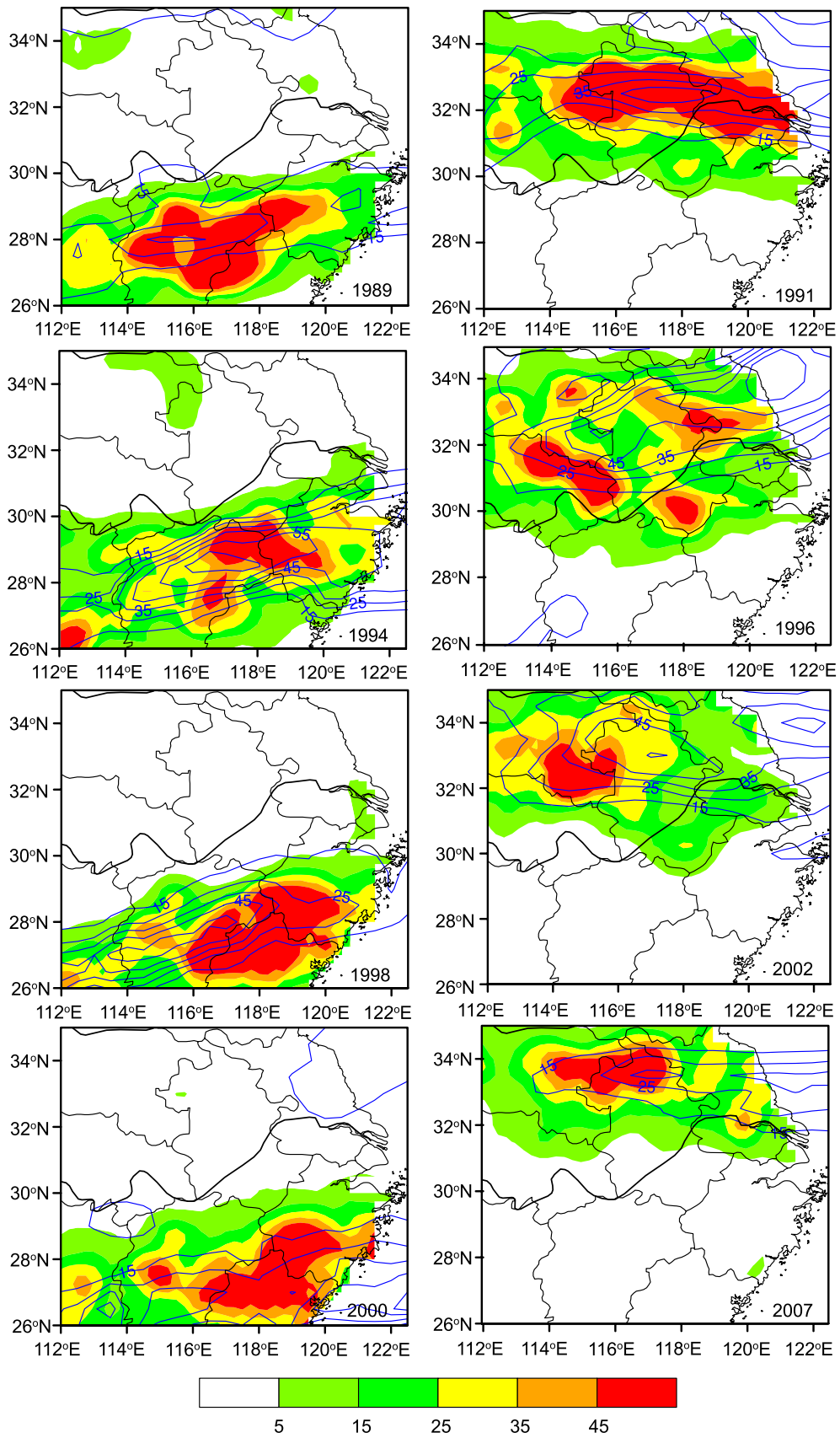
Fig. 1. The three-day total precipitation (color shading; units: mm) and the three-day time-averaged perturbation KE (blue contours; units: m^{-2} s^{-2}) of the three types of PHREs. The left (right) column is for the four type-A (type-B) events.
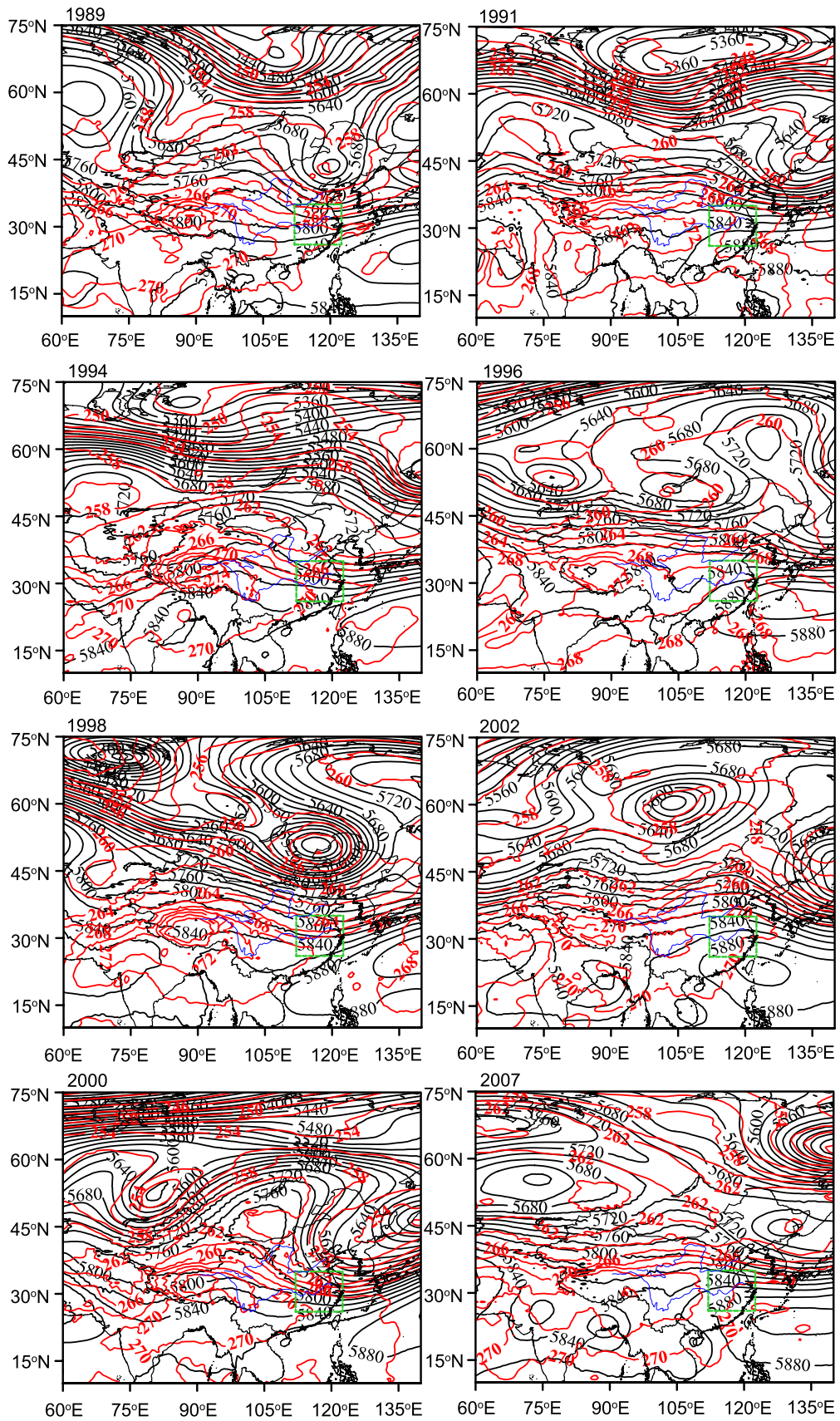
Fig. 2. Three-day averaged geopotential height (black contours; units: gpm) and temperature (red contours; units: K) at 500 hPa for type-A (left) and type-B (right) case. The green boxes in the figures symbolize our study area.
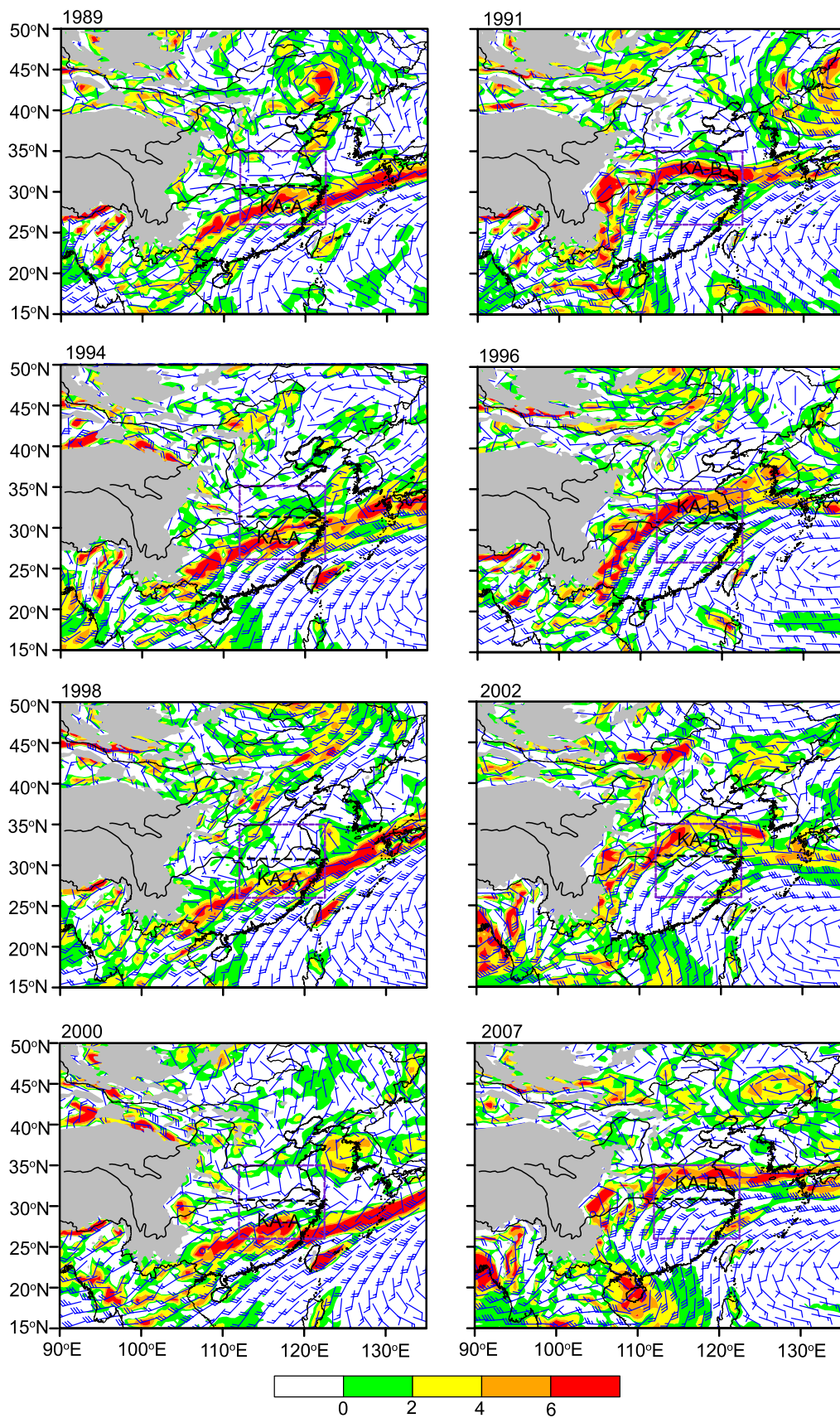
Fig. 3. Three-day averaged wind fields (blue wind barbs) and vorticity (> 0; color shading; units: 10^{-5} s^{-1}) at 850 hPa for type-A (left column) and type-B (right column) case. The purple boxes in the figures are the study areas. The grey shading represents the terrain higher than 1500 m.
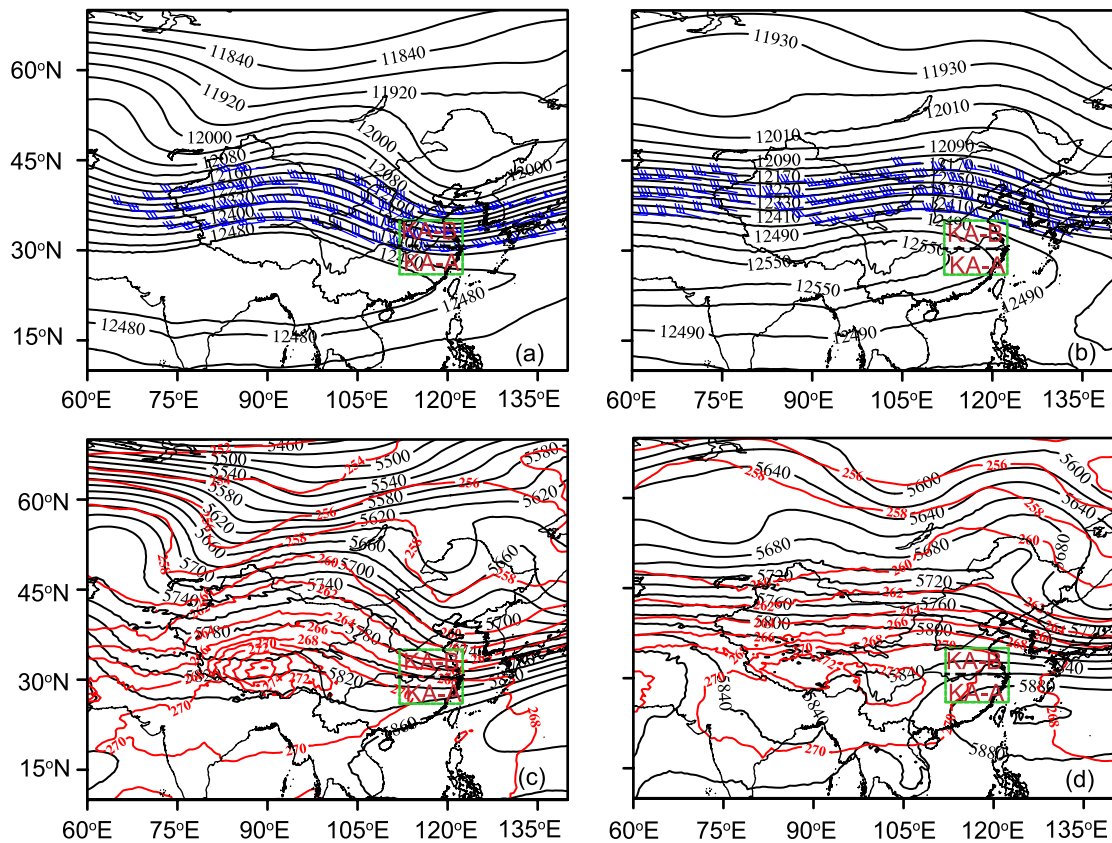
Fig. 4. (a, b) Composite averaged geopotential height (black contours; units: gpm) and jets (wind speed > 30 m s^{-1}; blue wind barbs) at 200 hPa: (a) the four type-A PHREs; (b) the four type-B PHREs. (c, d) Averaged geopotential height (black contours; units: gpm) and temperature (red contours; units: K) at 500 hPa: (c) the four type-A PHREs; (d) the four type B PHREs. The green rectangles are the key areas [northern side is the key area for type A (KA-A); southern side is the key area for type B (KA-B)] in this study.

this strong perturbation KE band was maintained could explain how the PHREs were sustained. The energy diagnostic scheme derived by Murakami (2011) was used to calculate the related energy characteristics (section 2.2).

To show the overall feature, the energy budget terms of Eqs. (1)–(4) were first averaged within the north box of the key area [KA-A; (26°–30°N, 112°–122.5°E)] for type-A PHREs, and within the south box [KA-B; (30°–34°N, 112°–122.5°E)] for type-B PHREs. Then, the horizontally averaged values were integrated vertically. The vertical integrals were calculated among three equal layers and the total layers. For the lower levels, the budget terms were integrated from 950 hPa to 700 hPa (950 hPa was used as the bottom level to avoid including information beneath the topography), the middle levels were integrated between 650 and 400 hPa, and the upper levels from 350 hPa to 100 hPa. The integration of the total levels started from 950 hPa and ended at 100 hPa.

4.1. *Energy features at different levels*

Integrated energy values during the three-day persistent precipitation period are shown in Fig. 6. To reflect the relative importance of the perturbation (precipitation-related eddy flow) regarding the mean state (mean flow and background

circulation), a ratio of K_T (A_T) divided by the sum of K_T (A_T) and K_M (A_M) was calculated, and was defined as the relative perturbation for KE (APE).

For the energy of the background circulation, the K_M maxima of the eight PHREs all appeared in the upper levels and decreased downward, which corresponded to the vertical configuration of the background circulation (Figs. 4 and 5). Generally, the K_M in the upper and middle levels of the four type-A events was larger than that in the four type-B events, whereas the K_M in the lower levels of the two types of PHREs showed little obvious difference. The A_M maximum of each PHRE also mainly appeared in the upper levels (except for the event in 1994), with the A_M values in the middle levels being slightly smaller than those in the upper levels. Similar to the differences in K_M between the type-A and -B PHREs, the A_M in the upper and middle levels was larger for the type-A PHREs, whereas the A_M in the lower levels was almost the same for the two types of PHREs. No obvious differences in the lower-level A_M and K_M between the type-A and type-B PHREs meant that the background circulations in the lower troposphere resembled each other, and provided favorable conditions for sustaining the precipitation-related eddy flow, which was mainly located in the lower troposphere (Fu
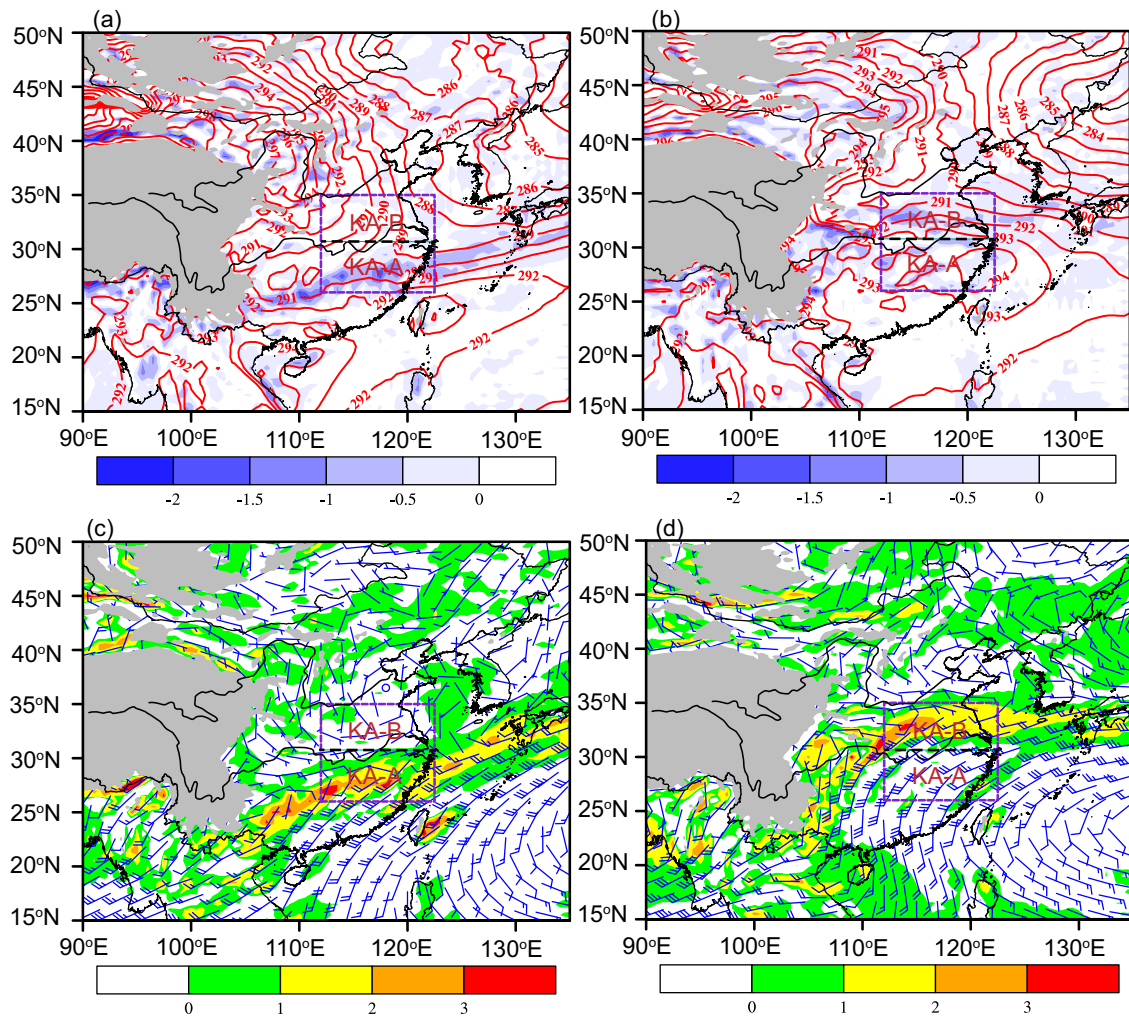
Fig. 5. (a, b) Composite averaged potential temperature (red contours; units: K) and divergence (< 0; color shading; units: 10^{-5} s^{-1}) at 850 hPa: (a) the four type-A PHREs; (b) the four type-B PHREs. (c, d) Averaged wind fields (blue wind barbs) and vorticity (> 0; color shading; units: 10^{-5} s^{-1}) at 850 hPa: (c) the four type-A PHREs; (d) the four type-B PHREs. The purple rectangles are the key areas [northern side is key area for type A (KA-A); southern side is key area for type B (KA-B)] in this study. The grey shading indicates terrain height > 1500 m.

et al., 2015).

For the perturbation energy, it was clear that, in all four layers, the relative perturbation of KE was generally larger for the type-B PHREs. This meant that the precipitation-related eddy flow in the type-B PHREs had stronger relative intensity. In contrast to the vertical distribution of K_M, the relative perturbation of KE reached a maximum in the lower levels and a minimum in the middle levels. The appearance of maximum relative perturbation of KE in the lower levels meant, dynamically, the precipitation was mainly triggered by lower-tropospheric systems. The relative perturbation of APE in all eight PHREs also peaked in the lower levels, which indicated that the maximum relative perturbation in the thermodynamical fields also appeared in the lower troposphere. The relative perturbation of APE was larger for type-B PHREs in the middle and upper levels, whereas the opposite was true for the lower levels.

4.2. *Energy paths of type-A events*

The energy features in the total levels were investigated to show the overall energy characteristics of the precipitation region, and the energy features in the lower levels were analyzed in detail as they were directly linked to the PHREs (Fig. 7). In the total levels, for the four type-A PHREs, the main energy paths of the background circulation were as follows. The baroclinic energy conversion (BCEC) from A_M to K_M dominated the maintenance of K_M. The transport effect $B(A_M)$ was the main factor favorable for the maintenance of A_M. The diabatic effect $G(A_M)$ and the vertical heat transport effect $R(A_M)$ also contributed to the persistence of A_M. For the eddy flow, $G(A_T)$ was dominant for the energy maintenance of A_T. A_T was produced by heating in warm regions or cooling in cold regions, while heating in cold regions or cooling in warm regions had the opposite effect. A_T was reduced by the BCEC of the eddy flow [i.e., $C(A_T, K_T) > 0$]. Mean-
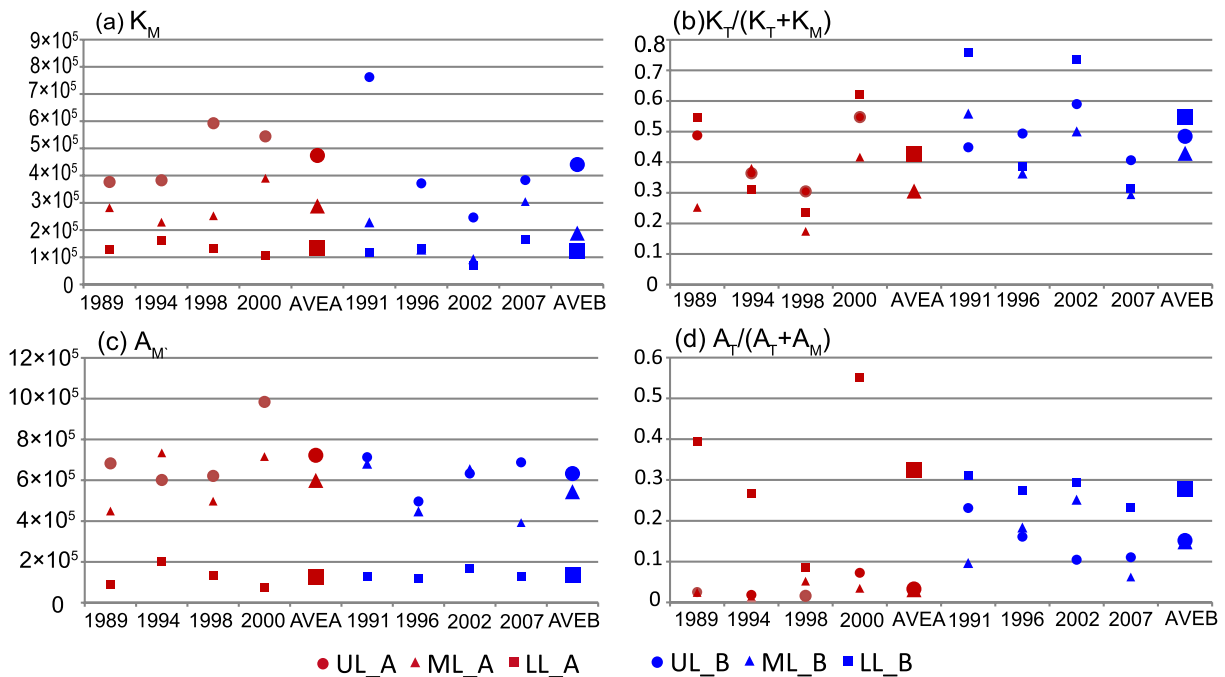
Fig. 6. The vertical integral of the key areas' averaged mean KE (KM), mean APE (AM), the relative perturbation KE (KT) and perturbation APE (AT). Red circles, triangles and squares are for the energy integrated for the upper levels (UL), middle levels (ML) and lower levels (LL) of type-A PHREs, and those with blue color are for the energy of type-B PHREs.

while, the BCEC was the main energy source for the sustainment of K_T. Within the precipitation region, a proportion of K_T was converted into K_I (except for the 2000 PHRE). The eddy transport $B(K_T)$ and the friction effect $D(K_T)$ also consumed K_T. A small part of A_M was transferred to A_I and then A_I was converted into A_T, which meant a downscaled ECP of APE appeared. This downscaled ECP of APE was the second dominant factor for maintaining A_T. A_I was primarily produced by interactions with the background circulation. K_I in the 1994 and 1998 PHREs was mainly generated by interactions with the eddy flow and background circulation, whereas the K_I of the 1989 PHRE received energy from K_T and converted the energy to K_M, i.e., an upscaled ECP, indicating KE was transferred from the eddy flow to its background circulation. In contrast, K_I in the 2000 case was mainly generated from interactions with the background circulation.

The energy paths in the upper levels (350 to 100 hPa, not shown) of the four events was similar to the corresponding path in the total levels. $B(A_M)$, $G(A_M)$ and $R(A_M)$ also contributed to the maintenance of A_M, with the BCEC process from A_M to K_M dominating the persistence of K_M. The downscaled ECP of APE appeared in three events (except for the PHRE in 1998), which was important for sustaining A_T, whereas the BCEC process converted a part of A_T to K_T, which reduced A_T. K_I was mainly generated through interactions with the eddy flow and background circulation (except for the 1989 event). The energy source of A_M and the BCEC processes from APE to KE (both background circulation and eddy flow) in the middle levels (650 to 400 hPa) were the same as those in the total levels. Unlike the significant downscaled ECP of APE in the total and upper levels,

there was no obvious ECP in the middle levels. Both A_M and A_T converted the energy to A_I and then most of A_I was transported out of KA-A by the eddy flow [$F(A_I) > 0$]. Both the background circulation and eddy flow converted KE to K_I through $C(K_M, K_I)$ and $C(K_T, K_I)$, respectively, in the PHREs of 1994 and 2000. For the PHREs of 1989 and 1998, an upscaled ECP, which transferred KE from the eddy flow to the background circulation, appeared, but it was negligible to the evolution of K_M.

Previous studies have demonstrated that, over the Yangtze River–Huaihe River valleys, the precipitation-related eddy flow is primarily maintained in the lower levels (950–700 hPa) (Tao, 1980; Zhao et al., 2004). The results of the present study confirm this result (maximum relative perturbation of APE and KE both appeared in the lower levels). Therefore, the energy paths in the lower levels could indicate the energy evolution of weather systems that are directly related to rainfall. In the lower levels, the energy paths and cascade processes were generally similar for the four PHREs. The similarities are summarized as follows. First, the diabatic effect $G(A_M)$ and the vertical heat transport effect $R(A_M)$ were both favorable for A_M persistence. Second, the BCEC from A_M to K_M was dominant for the maintenance of K_M, whereas the transport effects $B(K_M)$ and $D(K_M)$ were the main consumption factors for reducing K_M. Third, except for the PHRE in 2000, the BCEC of the eddy flow was from KE to APE, reducing the intensity of the eddy flow. This was the most significant difference in the energy path compared with other levels. Finally, remarkable downscaled ECPs of APE and KE appeared in the lower troposphere, showing that the background circulation acted as a crucial energy source for the
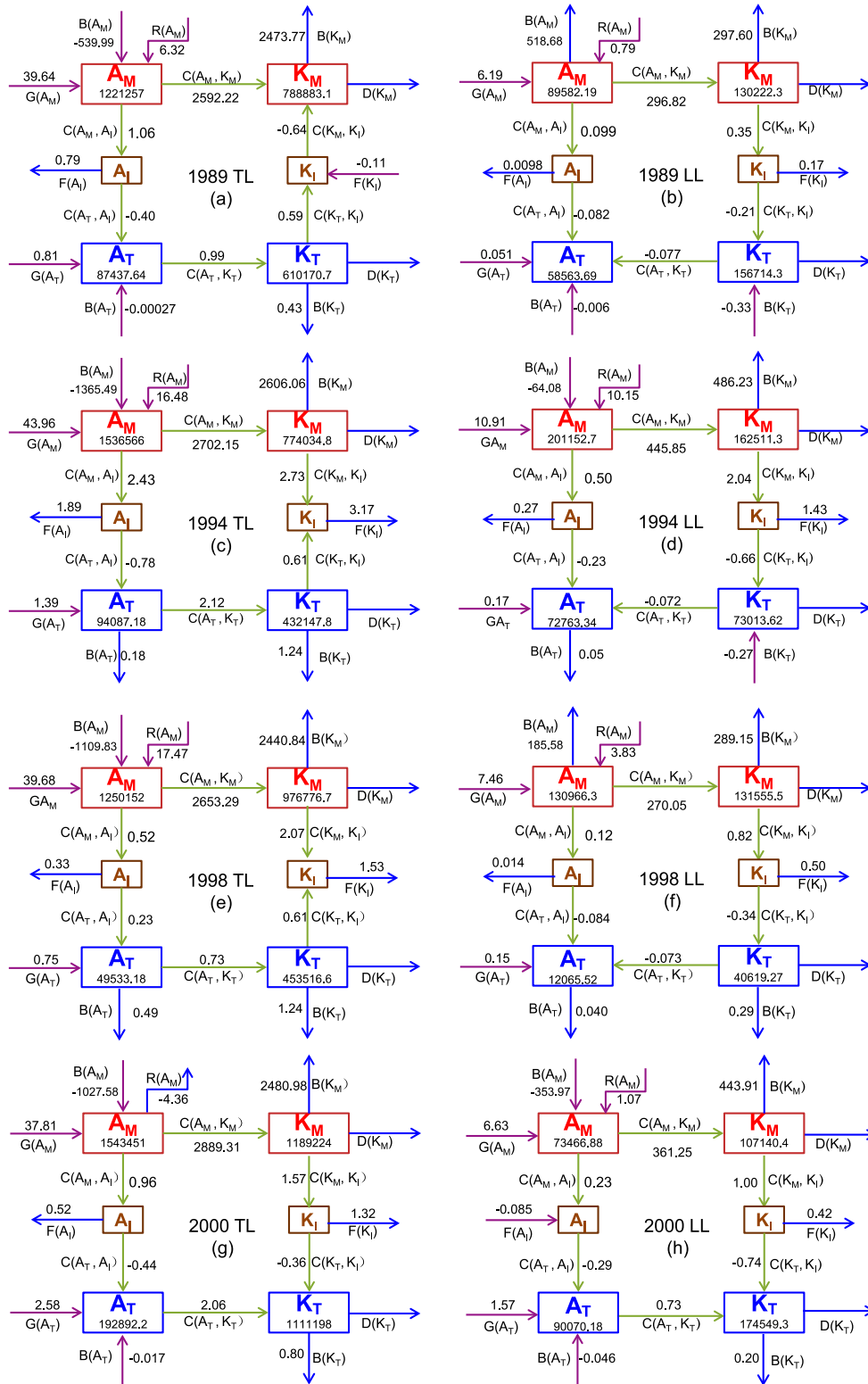
Fig. 7. Vertical integral of the area-averaged (26°–34°N, 122°–122.5°E) energy (units: J m^{-2}) and budget terms (units: W m^{-2}) at the different levels for type-A PHREs. A_M, A_I and A_T are the time-mean, interaction and perturbation APE; and K_M, K_I and K_T are the time-mean, interaction and perturbation KE. $G(A_M)$ and $G(A_T)$ are the diabatic generation or extinction of A_M and A_T. $C(X1, X2)$ represents the conversion between the energy $X1$ and energy $X2$. $D(A_M)$ and $D(A_T)$ denote the dissipation of K_M and K_T. $B(X)$ is the three-dimensional transport associated with X. $R(A_M)$ represents the vertical transport of heat.

precipitation-related eddy flow.

4.3. *Energy paths of type-B events*

The energy paths in the total levels of the type-B PHREs showed obvious similarities to the type-A PHREs (Fig. 8). First, for the background circulation, $B(A_M)$, $G(A_M)$ and $R(A_M)$ were favorable for the maintenance of A_M, with $B(A_M)$ acting as the dominant energy source. The BCEC from A_M to K_M was the main KE source for the background circulation. For the eddy flow, $G(A_T)$ mainly produced A_T (except for the 2002 PHRE). The BCEC of eddy flow converted energy from APE to KE, which dominated the persistence of K_T. The primary energy source of A_I was the interaction with the background circulation, and A_I was mainly converted into A_T, which was a downscaled ECP of APE. The downscaled ECP of KE only appeared in the PHREs of 1996 and 2002; whereas, in the other two PHREs, the generation of K_I was primarily from the interactions with both the eddy flow and the background circulation.

The energy path in the upper levels (not shown) was similar to that in the total levels. The transport effect $B(A_M)$ and the diabatic effect $G(A_M)$ were mainly conducive to the sustainment of A_M. The BCEC from $A_M(A_T)$ to $K_M(K_T)$ was the unique dominant energy source of background (eddy flow) KE. For the interaction energy, downscaled ECPs only appeared in the thermodynamical fields (APE). In contrast, both the background circulation and eddy flow transferred KE to K_I through $C(K_M, K_I)$ and $C(K_T, K_I)$, respectively (except for the 2007 PHRE). The BCEC of the background circulation and eddy flow in the middle levels were the same as those in the total levels; however, the ECPs of APE and KE were different (not shown). For the ECPs of KE, an upscaled ECP (energy conversion from K_T to K_M through K_I) appeared in the 1991 and 2007 PHREs.

For the energy paths and ECPs in the lower levels of the four type-B events, the main similarities can be summarized as follows (Fig. 8). First, $G(A_M)$ and $R(A_M)$ were favorable for the maintenance of A_M. The BCEC from APE to KE of the background circulation [$C(A_M, K_M) > 0$] was the unique dominant energy source for the sustainment of K_M. The second common feature was that the BCEC from A_T to K_T, favorable for the development of the precipitation-related weather systems, appeared (except for the PHRE of 1996). Third, downscaled ECPs appeared both in APE and KE. The background circulation transferred energy (APE and KE) into the precipitation-related eddy flow through the interaction energy.

4.4. *Comparison of energy cascade processes in type-A and -B events*

The differences and similarities between the two types of PHREs are discussed in this section. As described in section 3.1, comparison of the KE and APE associated with the background circulation showed that the type-A PHREs (rainbelt located south of the Yangtze River) were generally stronger than the type-B PHREs at all levels. One possible reason is that, compared with the type-B PHREs, the type-A

PHREs appeared in warmer regions with a stronger upper-level jet and low-level jet (Figs. 4 and 5). For both types of PHREs, the KE and APE reached a maximum in the lower troposphere, because the weather systems directly triggering a PHRE (shear line, front, convergent line, etc.) were mainly located in the lower levels. The K_T of the type-B PHREs was stronger than that of the type-A PHREs, whereas the A_T of the type-A PHREs was larger. This indicates that, dynamically, the eddy flow accounting for the type-B PHREs was more intense; whereas, thermodynamically, the precipitation-related eddy flow in type-A PHREs had stronger baroclinicity.

The layer-based energy paths of the two types of PHREs are summarized in Fig. 9. The common and universal energy paths of the two types of PHREs can be summarized as follows. For the APE of the background circulation, diabatic generation [$G(A_M)$] was the main energy source for A_M at all levels. The BCEC process from A_M to K_M was dominant for the sustainment of K_M. The $B(K_M)$ and $D(K_M)$ were the main factors for the consumption of K_M. A proportion of A_M was transferred to A_T via the interaction energy (A_I) (except for in the middle troposphere), which was the downscaled ECP of APE. For the KE of the precipitation-related eddy flow, the BCEC from A_T to K_T was the main energy source for its persistence in the upper and middle troposphere. Significant downscaled ECPs of KE appeared in the lower troposphere, which sustained the precipitation-related eddy flow directly.

The main differences in the energy paths of the two types of PHREs appeared in the lower troposphere. The BCEC of eddy flow in the type-A PHREs was mainly from KE to APE, which resulted in larger A_T south of the Yangtze River. However, this conversion meanwhile reduced the intensity of K_T. In contrast, the BCEC of the type-B PHREs was mainly from APE to KE, which resulted in stronger K_T north of the Yangtze River.

5. Conclusion and discussion

Based on the classification of PHREs from Wang et al. (2014), four type-A (main rainbelt south of the Yangtze River) and four type-B (main rainbelt north of the Yangtze River) PHREs, all of which lasted for a three-day period, were selected for energy budget calculations. The energy budget was calculated using a recently introduced set of energy equations based on temporal scale separation. Through these energy analyses, the energy paths that sustained the two types of PHREs were determined, and the main results were as follows.

Owing to the differences in the vertical configuration of the background circulation, although A_M and K_M reached a maximum in the upper troposphere and decreased downward, the type-A PHREs generally had stronger A_M and K_M than the type-B PHREs. The two main similarities in the energy paths of the two types of PHREs were: (1) the BCEC from the APE to KE was the dominant energy source for the evolution of background circulation at all levels; and (2) the downscaled ECPs of KE and APE were vital in the evolution of the eddy flow, which directly triggered the PHREs. The
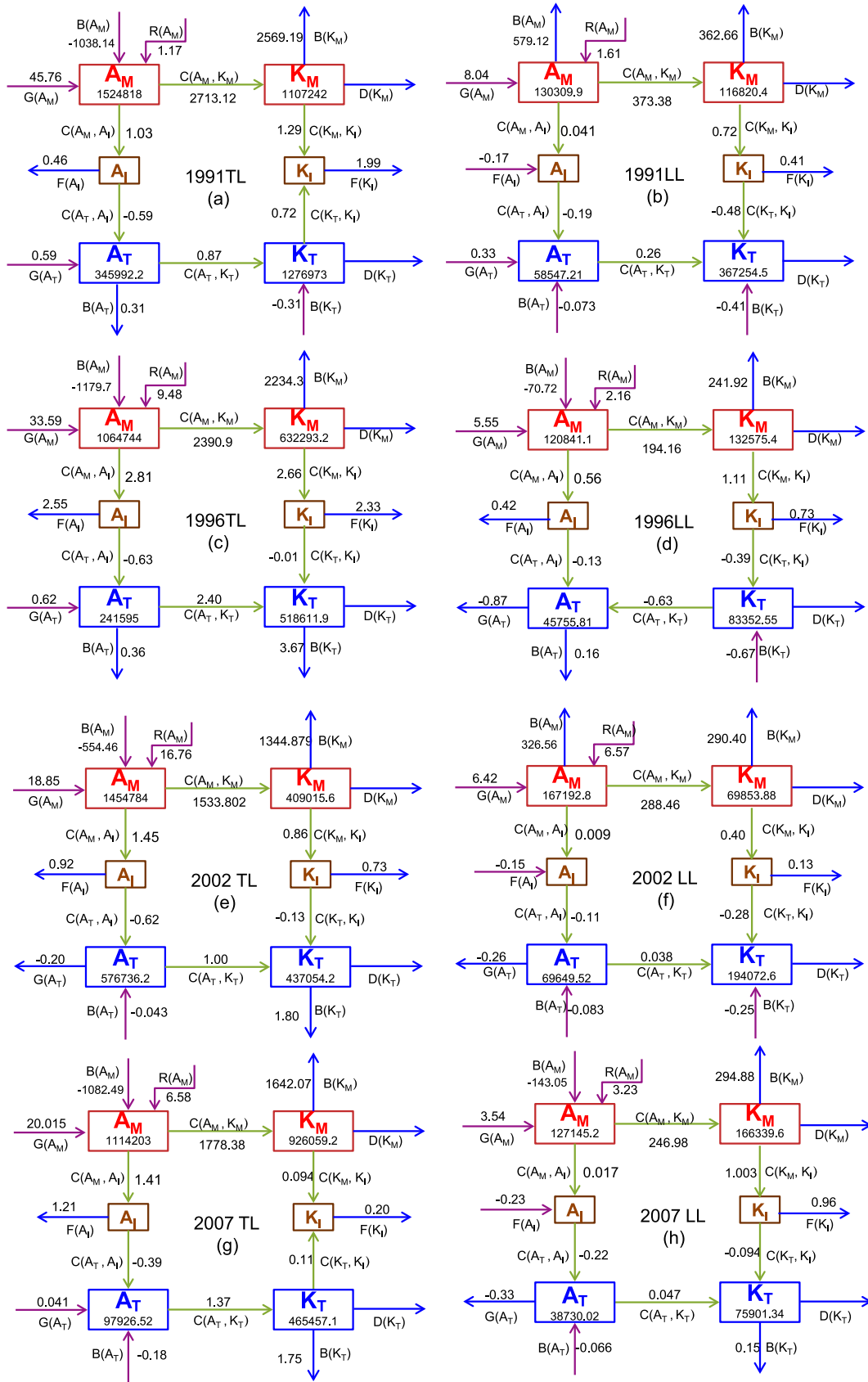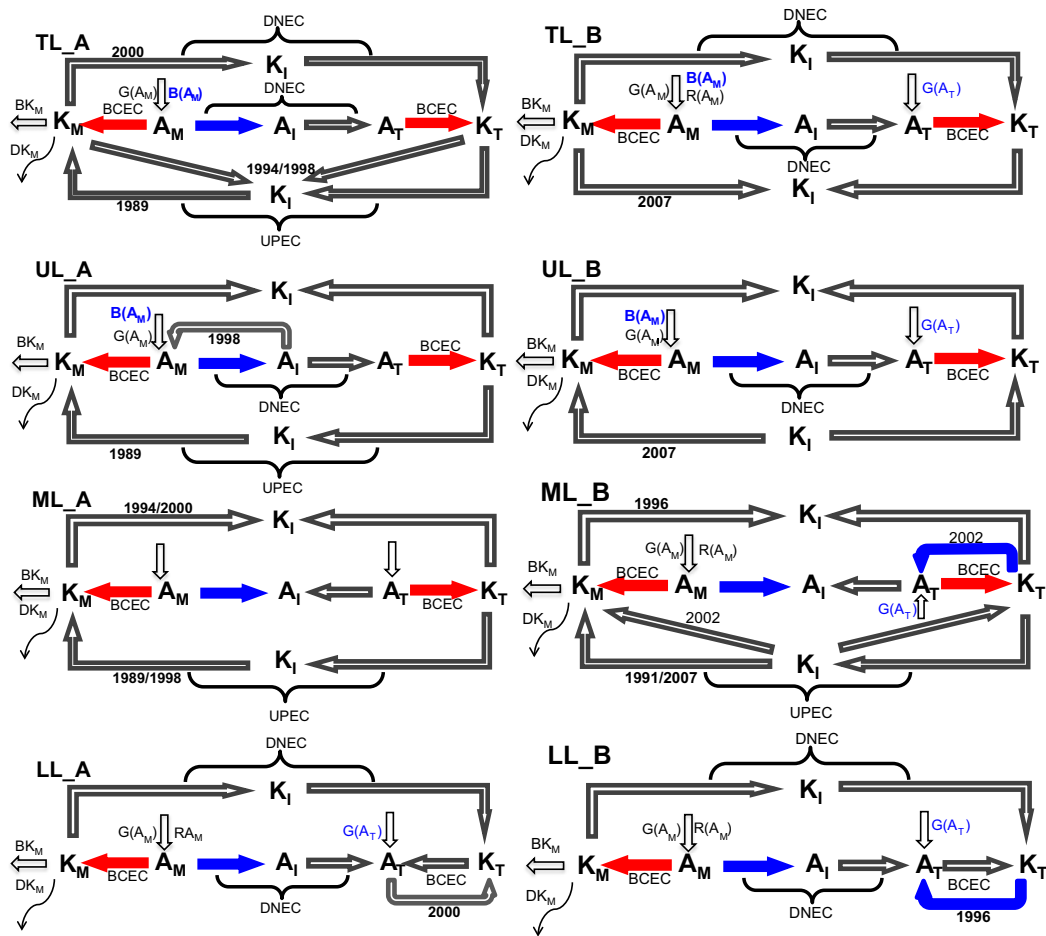
Fig. 8. As in Fig. 7, but for type-B PHREs.

Fig. 9. Main energy paths in the different levels for type–A PHREs (left column, TL_A, UL_A, ML_A and LL_A means the energy path of type-A integrated at total levels, upper levels, middle levels and lower levels.) and type-B PHREs (right column, TL_B, UL_B, ML_B and LL_B means the energy path of type-B integrated at total levels, upper levels, middle levels and lower levels.). $D(K_M)$ denotes the dissipation of K_M. $B(K_M)$ is the three-dimensional transport associated with X. BCEC is short for baroclinic energy conversion; DNEC means downscaled energy cascade and UPEC is upscaled energy cascade.

significant differences in the energy paths of the type-A and -B PHREs mainly appeared in the lower troposphere. The BCEC processes associated with the precipitation-related eddy flow in type A PHREs was from KE to APE, which reduced the intensity of K_T south of the Yangtze River. In contrast, the BCEC processes of the type-B PHREs were mainly from APE to KE, which enhanced K_T north of the Yangtze River.

Additionally, another set of four three-day cases were selected to composite the energy paths of the type-C PHREs (Fig. 10). Similar to the former two types of PHREs, the diabatic generation $G(A_M)$ was the main energy source for the APE of the background circulation (A_M) at all levels, except one PHRE in 1996. The BCEC process from A_M to K_M was also the main source for the sustainment of K_M. Moreover, another similarity was the downscaled ECP of APE appeared in the lower and upper levels instead of the middle troposphere. The BCEC from A_T to K_T was also the main energy source for the persistence of the KE of the precipitation-related eddy flow in the upper and middle tro-

posphere. Different from the significant variety of the type-A and -B PHREs, type C had more consistent downscaled ECPs of KE, which appeared in the lower to middle troposphere. As explained in the above sections, the BCEC of eddy flow in the type-A PHREs was mainly from KE to APE, but the BCEC of the type-B PHREs was mainly from APE to KE. The type C PHREs showed hybrid features between type A and B: the eddy flow of the two cases of type-C PHREs received its KE from APE through BCEC, while a reverse BCEC from KE to APE appeared in the other two cases.

The present study primarily focused on and explored the main energy paths of two types (type A and type B) of PHREs over the Yangtze River–Huaihe River basin—particularly the interactions between the precipitation-related eddy flow and its background circulation. As discussed in section 2.2, this background circulation is a combined system that includes various signals of different temporal scale (in this study, the three-day running mean made the background circulation only have signals with periods larger than three days). In fact, each of the signals in the background circulation has an
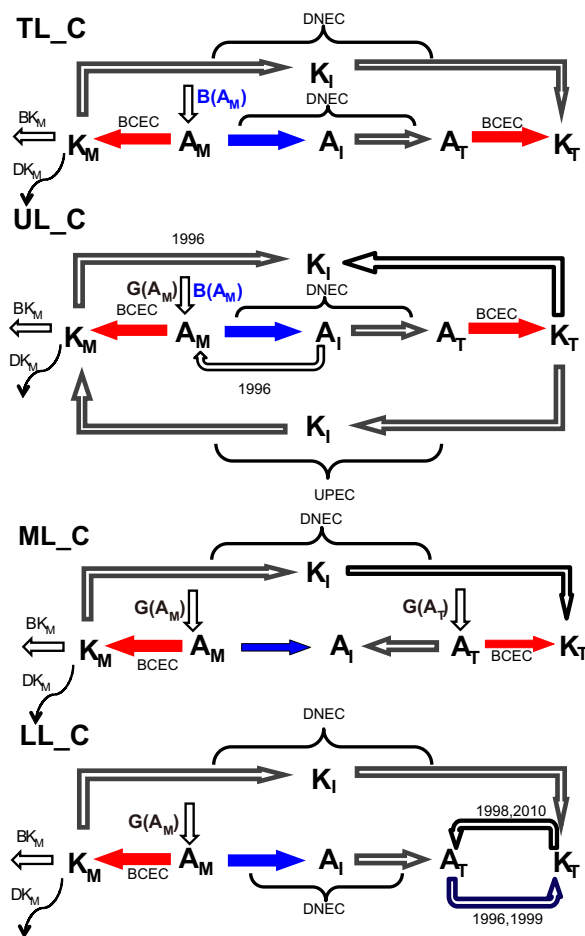
Fig. 10. Main energy paths in the different levels for type-C PHREs. TL_C, UL_C, ML_C and LL_C means the energy path of type-C integrated at total levels, upper levels, middle levels and lower levels.

impact on the precipitation-related eddy flow, and the feedback from the eddy flow also affects the signals in the background circulation. Therefore, further studies should be conducted to determine the dominant background circulation signal for a PHRE. This would be useful for the forecasting and understanding of PHREs. In future work, these knowledge gaps will be addressed by applying the frequency-power analysis and filter method to the energy budget system of Murakami (2011).

REFERENCES

Chen, S. J., L. S. Bai, and E. C. Kung, 1990: An approach to kinetic energy diagnosis of meso-synoptic scale interactions. *Mon. Wea. Rev.*, **118**, 2774–2780.

Ding, Y. H., 1993: *Study of Strong Heavy Rianfall in Yangtze-Huai River in 1991*. China Meteorological Press, Beijing, 1–255. (in Chinese)

Fu, S. M., J. H. Sun, S. X. Zhao, and W. L. Li, 2011: The energy budget of a southwest vortex with heavy rainfall over South China. *Adv. Atmos. Sci.*, **28**(3), 709–724, doi: 10.1007/s00376-010-0026-z.

Fu, S. M., F. Yu, D. H. Wang, and R. D. Xia, 2013: A comparison of two kinds of eastward-moving mesoscale vortices during the mei-yu period of 2010. *Science China Earth Sciences*, **56**, 282–300.

Fu, S. M., W. L. Li, and J. Ling, 2015: On the evolution of a long-lived mesoscale vortex over the Yangtze River Basin: Geometric features and interactions among systems of different scales. *J. Geophys. Res. Atmos.*, **120**, 11 889–11 917, doi: 10.1002/2015JD023700.

Fu, S. M., J. H. Sun, J. Ling, H. J. Wang, and Y. C. Zhang, 2016: Scale interactions in sustaining persistent torrential rainfall events during the Mei-yu season. *J. Geophys. Res.* Atmos., 121, doi: 10.1002/2016JD025446.

Guo, S. L., F. Ge, R. Ma, L. Tian, and L. Zhou, 2012: Analysis of the accumulation and propagation of wave packets during a heavy rainfall process in southern China. *Journal of Tropical Meteorology*, **28**(4), 585–593 (in Chinese).

Holopainen, E. O., 1978: A diagnostic study on the kinetic energy balance of the long-term mean flow and the associated transient fluctuation in the atmosphere. *Geophysica*, **15**, 125–145.

Li, T. T., and X. F. Li, 2016: Barotropic processes associated with the development of the Mei-yu precipitation system. *Adv. Atmos. Sci.*, **33**(5), 593–598, doi: 10.1007/s00376-015-5146-z.

Li, Y. F., 2007: Conversion of kinetic energy from synoptic scale disturbance to low-frequency fluctuation over the Yangtze River valley in the summers of 1997 and 1999. *Adv. Atmos. Sci.*, **24**(4), 591–598, doi: 10.1007/s00376-007-0591-y.

Murakami, S., 2011: Atmospheric local energetics and energy interactions between mean and eddy fields. Part I: Theory. *J. Atmos. Sci.*, **68**, 760–768.

Murakami, S., R. Ohgaito, and A. Abe-Ouchi, 2011: Atmospheric local energetics and energy interactions between mean and eddy fields. Part II: An example for the Last Glacial Maximum climate. *J. Atmos. Sci.*, **68**, 533–552.

Plumb, R. A., 1983: A new look at the energy cycle. *J. Atmos. Sci.*, **40**, 1669–1688.

Ritchie, E. A., and G. J. Holland, 1997: Scale interactions during the formation of Typhoon Irving. *Mon. Wea. Rev.*, **125**, 1377–1396.

Saha, S., and Coauthors, 2010: The NCEP climate forecast system reanalysis. *Bull. Amer. Meteor. Soc.*, **91**, 1015–1057, doi: 10.1175/2010BAMS 3001.1.

Tang, Y. B., J. J. Gan, L. Zhao, and K. Gao, 2006: On the climatology of persistent heavy rainfall events in China. *Adv. Atmos. Sci.*, **23**(5), 678–692, doi: 10.1007/s00376-006-0678-x.

Tao, S. Y., 1980: *Heavy Rainfall Events in China*. Science Press, Beijing, 45–46 (in Chinese).

Tao, S. Y., and S. Xu, 1962: Some aspects of the circulation during the periods of the persistfnt drought and flood in Yantze and Hwai-ho valleys in summer. *Acta Meteorologica Sinica*, **32**(1), 1–10 (in Chinese).

Tao, S. Y., Y. Q. Ni, S. X. Zhao, S. J. Chen, and J. J. Wang, 2001: *The Study on Formation Mechanism and Forecasting of Heavy Rainfall in the Summer 1998*. China Meteorological Press, 183–184 (in Chinese).

Tao, S. Y., X. L. Zhang, and S. L. Zhang, 2004: *A Study on the Dis-*

aster of Heavy Rainfalls over the Yangtze River Basin in the Meiyu Period. China Meteorological Press, 192 pp (in Chinese).

Wang, H. J., J. H. Sun, J. Wei, and S. X. Zhao, 2014: Classification of persistent heavy rainfall events over southern China during recent 30 years. *Climatic and Environmental Research*, **19**(6), 713–725 (in Chinese).

Xu, Y. F., 2008: The spatial-temporal variation of persistent heavy rainfall in south of China in summer and its corresponding general circulation feature. M. S. thesis, Nanjing University of Science and Technology, 8–46 (in Chinese).

Zhao, S. X., Z. Y. Tao, J. H. Sun, and N. F. Bei, 2004: *Study on Mechanism of Formation and Development of Heavy Rainfalls on Meiyu front in Yangtze River*. China Meteorological Press, 282 pp (in Chinese).